Bismuth Telluride (Bi2Te3) Nanowires Synthesized by Cyclic Electrodeposition/Stripping Coupled with Step Edge Decoration

ARTICLE *in* NANO LETTERS · SEPTEMBER 2004

Impact Factor: 13.59 · DOI: 10.1021/nl048627t

3 AUTHORS, INCLUDING:

Erik Menke
University of California, Merced
18 PUBLICATIONS **1,021** CITATIONS

SEE PROFILE

NANO LETTERS

2004
Vol. 4, No. 10
2009−2014

Bismuth Telluride (Bi_2Te_3) Nanowires Synthesized by Cyclic Electrodeposition/Stripping Coupled with Step Edge Decoration

E. J. Menke, Q. Li, and R. M. Penner*

Department of Chemistry, University of California, Irvine, California 92697-2025

Received August 24, 2004; Revised Manuscript Received August 30, 2004

ABSTRACT

Polycrystalline bismuth telluride (Bi_2Te_3) nanowires have been prepared by the step edge selective electrodeposition of Bi_2Te_3 on highly oriented pyrolytic graphite (HOPG) surfaces. Bi_2Te_3 nanowires were obtained from an aqueous plating solution containing Bi^{3+} and $HTeO_2^+$ using a three-step procedure: (1) potentiostatic oxidation of the graphite surface at +0.8 V (vs saturated calomel electrode, SCE), (2) potentiostatic nucleation of Bi_2Te_3 at −0.6 V for 5 ms, (3) growth of Bi_2Te_3 from these nuclei by cyclic electrodeposition (of both Bi_2Te_3 and bismuth) and stripping (of bismuth only) between +0.30 V and −0.05 V at 20 mV s^{-1}. Control of the number of electrodeposition/stripping scans allowed the diameter of Bi_2Te_3 nanowires to be specified in the range from 100 to 300 nm. Bi_2Te_3 nanowires were narrowly dispersed in diameter (RSD_{dia} = 10–20%), were up to 1.0 mm in length, and were organized into parallel arrays containing hundreds of wires.

Thermoelectric (TE) generators produce electrical power from a temperature gradient. The efficiency of a particular thermoelectric material for power generation can be expressed in terms of the dimensionless quantity ZT[1]:

$$ZT = \frac{S^2\sigma T}{\kappa} \quad (1)$$

where Z is the thermoelectric figure of merit, T is the mean temperature of the material, S is the thermoelectric power or Seebeck coefficient, σ is the electrical conductivity, and κ is the thermal conductivity. The best thermoelectric materials at room temperature are members of the $Bi_{2(1-x)}Sb_{2x}$-$Te_{3(1-y)}Se_{3y}$ family and possess a $ZT \approx 1$ near room temperature (300−450 K).[1] Theoretical investigations have suggested that low-dimensional materials may exhibit ZT values considerably larger than 1.0 as a consequence of enhanced S and σ,[2−6] and/or depressed κ[7−12] relative to the corresponding properties of bulk material.

These predictions have stimulated interest in the synthesis of Bi_2Te_3 nanowires. Until now template synthesis[13−15] has been exclusively used to obtain Bi_2Te_3 nanowires by both Martin[16] and Stacy[17−19] who electrodeposited Bi_2Te_3 into the pores of a porous alumina membrane. Both research groups employed an electrodeposition recipe similar to that originally described by Magri et al.:[20]

$$2Bi^{3+} + 3HTeO_2^+ + 3H_2O + 18e^- \rightleftharpoons Bi_2Te_3 + 9OH^- \quad (2)$$

Nanowires with minimum diameters of 280 and 40 nm, respectively, were obtained by these two research groups, whereas the lengths of the nanowires prepared by template synthesis range from 10 to 50 μm.

Efficient thermoelectric devices are likely to require nanowires that are not only extremely narrow but also extremely long − in excess of 50 μm. Min and Rowe[1,21−23] have derived equations that allow performance metrics (power, efficiency, etc.) to be calculated for two-element Peltier devices, like that shown in Figure 1a. These equations include a consideration of the properties of the electrical and thermal contacts. One important metric is the electrical power generated by such a device:[1]

$$P = \frac{\pi r^2 (S\Delta T)^2}{\rho L_o (1 + (2\rho_c/\rho L_o))(1 + (2\kappa L_c/\kappa_c L_o))^2} \quad (3)$$

where ΔT is the temperature difference measured at the external surfaces of the ceramic layers, r is the radii of the two cylindrical thermoelements, ρ is the electrical resistivity

* Corresponding author. E-mail: rmpenner@uci.edu.

10.1021/nl048627t CCC: $27.50
Published on Web 09/14/2004

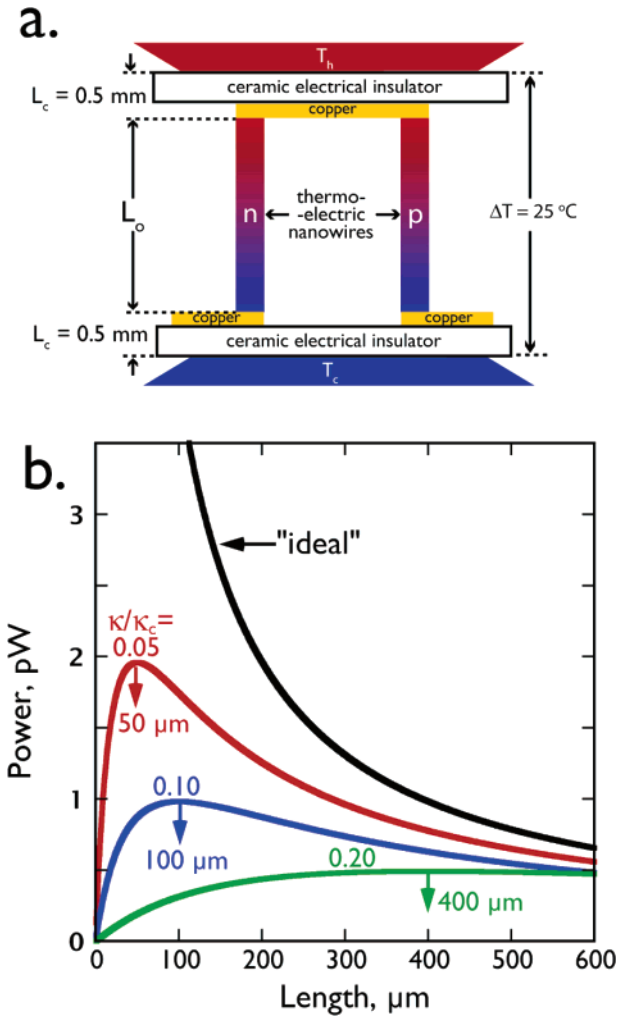

Figure 1. (a) Schematic diagram of a two-element thermoelectric device showing parameters contained in eq 3. (b) Plot of total power generated, P, from the device shown in (a) as a function of the nanowire length, L_o. Shown are plots for three values of the ratio κ/κ_c as indicated. Arrows mark the optimum nanowire length for each value of κ/κ_c. The values of the other parameters indicated in eq 2 are as follows: $r = 10 \times 10^{-6}$ mm, $S = 2.00 \times 10^{-4}$ μV/K, $\Delta T = 25$ K, $\rho_c = 7$ kΩ, $\rho = 0.01$ Ω, and $L_c = 0.5$ mm (taken from ref 1). The power generated by a device with ideal contacts, indicated by the black trace, is: $P_{ideal} = (\pi r^2 (S\Delta T)^2/2\rho L_o)$.

of the nanowires with length L_o and thermal conductivity κ, and ρ_c is the electrical resistance of the contacts of total thickness (insulator + conductor) L_c, having a net thermal conductivity κ_c. When realistic values[24] are substituted for these parameters, the effect of nanowire length can be assessed. For example, the dependence of L_o on P is plotted in Figure 1b for three different values of the ratio κ/κ_c (0.05, 0.1, and 0.2). Figure 1b shows that P is maximized for nanowires that are 50 μm in length (for $\kappa/\kappa_c = 0.05$) or longer ($\kappa/\kappa_c > 0.05$) and that P falls rapidly with decreasing nanowire length below these optimum values. The plots of Figure 1b were calculated for nanowires with a diameter of 10 nm, but the optimum nanowire lengths, indicated by the arrows, are identical across the diameter range from 1 to 100 nm. Since a value of $\kappa/\kappa_c = 0.10$ is typical for state-of-the-art devices,[23] we conclude that nanowires longer than any synthesized to date may be required for device applications.

In this letter we describe a method for preparing arrays of hundreds of Bi_2Te_3 nanowires that are 100−300 nm in diameter and up to 1 mm in length. This method, a variant of the electrochemical step edge decoration (ESED) method developed in our lab,[25−31] involves the electrodeposition of Bi_2Te_3 selectively at the step edges present on a graphite surface, as shown schematically in Figure 2a. The potential program for our method is shown in Figure 2b and consists of three steps: (1) mild oxidation of the basal plane step edges on a piece of highly oriented pyrolytic graphite (HOPG) at +0.80 V for 5 s; (2) nucleation of nanoscopic Bi_2Te_3 particles along the oxidized step edges at −0.60 V for 5 ms; (3) co-deposition of Bi_2Te_3 and excess bismuth during a negative-going potential scan from +0.3 to −0.05 V and subsequent anodic stripping of excess bismuth, producing a stoichiometric Bi_2Te_3 deposit, during a positive-going potential scan from −0.05 V to 0.30 V. Step 3 is then repeated a number of times ("n" in Figure 2b) until the Bi_2Te_3 particles grow large enough to coalesce, forming continuous Bi_2Te_3 nanowires. This cyclic electrodeposition/stripping strategy is identical in concept to the method described by Sailor[32] for the electrodeposition of stoichiometric thin films of CdSe.

The electrochemical deposition of Bi_2Te_3 was carried out in a 50 mL, one-compartment, glass and Teflon three-electrode cell. The plating solution consisted of 1.5 mM bismuth(III) nitrate pentahydrate (Aldrich, 99.999%) and 1 mM tellurium oxide (Aldrich, 99.999%) in 1 M nitric acid prepared according to the published procedure.[20] This plating solution was prepared using Nanopure water ($\rho > 17.6$ MΩ) and was purged with N_2 prior to each experiment. A saturated calomel reference electrode (SCE) and a 2 cm^2 Pt foil counter electrode were also employed. The working electrode for these electrodeposition experiments was the basal plane surface of ZYA or ZYB grade HOPG crystals from GE Advanced Ceramics Inc. (Cleveland, OH). The basal plane surface was cleaved with adhesive tape prior to use, and a circular area of 0.2 cm^2 of was exposed, using an O-ring, to this plating solution. After deposition, the HOPG working electrode was removed from solution, rinsed with Nanopure water, and air-dried prior to characterization. Scanning electron microscopy (SEM) images and energy-dispersive X-ray fluorescence (EDX) analyses were acquired on a Philips Model XL-30FEG operating at 20 kV. Samples were mounted on aluminum SEM stubs using adhesive carbon dots from Ted Pella. Powder X-ray diffraction (XRD) spectra were acquired on a Siemens D5000 diffractometer operating at 40 keV and 30 mA. Transmission electron microscopy (TEM) and selected area electron diffraction (SAED) data were acquired on a Philips model CM20 operating at 200 kV.

Cyclic voltammograms (CVs) for a Bi_2Te_3 plating solution (Figure 2c) show a cathodic deposition peak at approximately

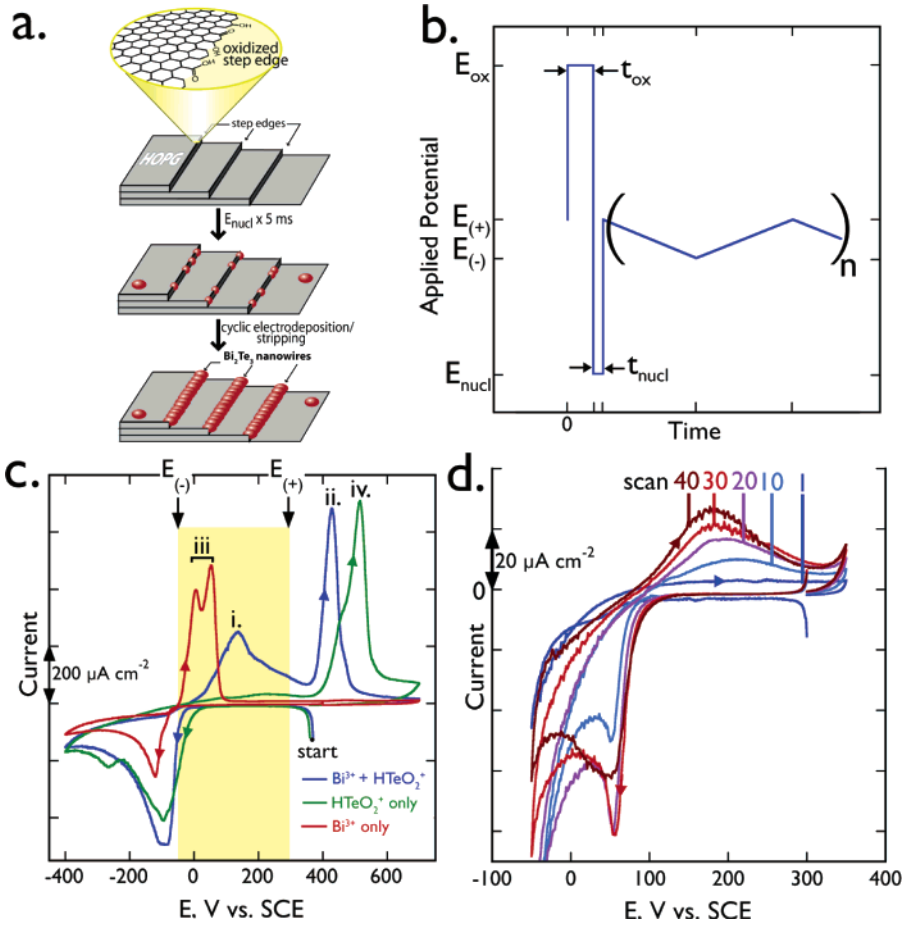

Figure 2. (a) Schematic diagram of the three-step method employed here for synthesizing Bi_2Te_3 nanowires by cyclic electrodeposition/stripping coupled with ESED. (b) Potential program, plotted as potential versus time, used for the synthesis by cyclic electrodeposition/stripping of Bi_2Te_3 nanowires. The electrodeposition of Bi_2Te_3 consisted of three steps: (1) potentiostatic oxidation of step edges on the HOPG surface at $E_{ox} = 0.80$ V vs SCE for a time $t_{ox} = 5$ s; (2) potentiostatic nucleation of Bi_2Te_3 at $E_{nucl} = -0.6$ V for $t_{nucl} = 5$ ms; and, (3) cyclic electrodeposition of stoichiometric Bi_2Te_3 involving n potential cycles at 20 mV s^{-1} between a positive limit of $E_{(+)}$ (+0.30 V) and a negative limit of $E_{(-)}$ (−0.05 V). (c) Cyclic voltammograms, CVs, for the HOPG basal plane in contact with the plating solution employed for Bi_2Te_3 nanowire growth (blue line). This solution contained: 1.5 mM $Bi(NO_3)_3$ and 1.0 mM TeO, in 1 M HNO_3. Also shown are CVs acquired in plating solutions containing just Bi^{3+} (red line) and just TeO_2^+ (green line). (d) CVs acquired during the growth of Bi_2Te_3 nanowires using cyclic electrodeposition/stripping. The scan number, n, is indicated at top.

−0.1 V, as well as two anodic peaks at +0.175 V (peak i) and +0.425 V vs SCE (peak ii). CVs of 1.5 mM Bi^{3+} in 1 M HNO_3 and 1 mM $HTeO_2^+$ in 1 M HNO_3 (Figure 2c) suggest that the broad anodic peak at +0.175 V can be assigned to the stripping of excess bismuth from a bismuth-rich Bi_2Te_3 deposit. These CVs also suggest that the anodic peak at +0.425 V is the stripping of Bi_2Te_3, not Te stripping, as this occurs at a potential (peak iv) more than 100 mV positive of this. These assignments, which are identical to those of Stacey et al.,[17] are also supported by EDX elemental analysis of the electrodeposits formed in each solution. One departure from the observations of Stacey et al.[17] concerns the potential at which the deposition of Bi_2Te_3 commences. In our case, this onset is at −50 mV and is well negative of the onset for tellurium deposition at 0.00 V; exactly the opposite was reported by Stacy et al.[17] for experiments conducted at platinum electrodes. The explanation, we believe, is the presence at the HOPG electrode of large nucleation overpotentials that are absent, or insignificant, at polycrystalline platinum electrodes. The existence of this nucleation overpotential for Bi_2Te_3 is exposed by the CVs recorded during Bi_2Te_3 deposition (Figure 2d) which show a prompt +80−100 mV shift in the Bi_2Te_3 deposition onset, accompanied by a dramatic sharpening of the cathodic wave at +60 mV, after just one deposition scan. The deposition CVs of Figure 2d show a second cathodic process occurring in the potential range from +0.02 V to −0.05 V, and this is assigned, based on EDX analysis, to the electrodeposition of pure bismuth, which is subsequently stripped (peak i) on the anodic return scan. We demonstrate below that the cyclic electrodeposition of Bi_2Te_3 provides a robust method for the production of near-stoichiometric Bi_2Te_3 wires.

Low magnification SEM images (Figure 3a) confirm that Bi_2Te_3 nanowires, and nanoparticles, are formed by the cyclic electrodeposition/stripping procedure detailed above. The nanowires are formed at step edges present on the HOPG surface, and both the step edges and the Bi_2Te_3 nanowires

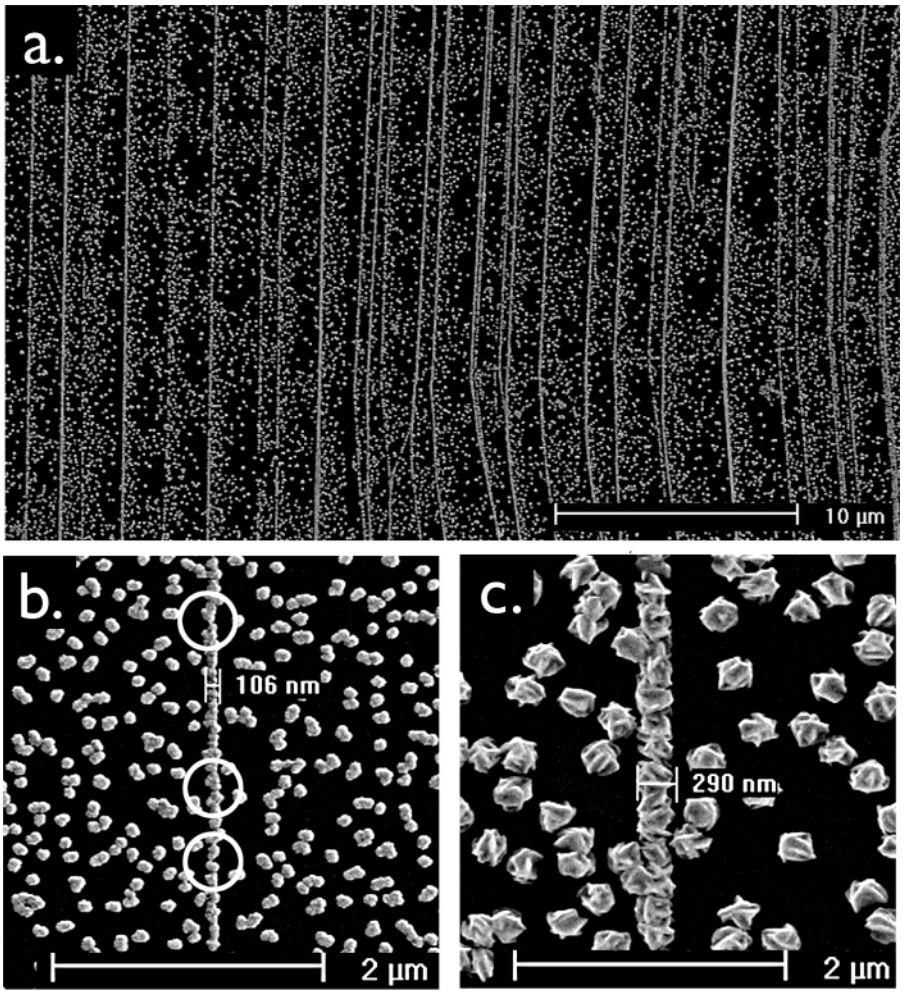

Figure 3. (a) Low magnification scanning electron microscope (SEM) image of Bi_2Te_3 nanowires prepared by cyclic electrodeposition/stripping. Bi_2Te_3 nanowires that nucleate and grow on step edges are arranged in parallel arrays. These nanowires are up to 1 mm in length. (b) High magnification SEM image of Bi_2Te_3 nanowires prepared using 10 electrodeposition/stripping cycles. The mean, outermost diameter of these nanowires is 115 nm; however, such wires are characterized by periodic constrictions, indicated by circles, that are 20 nm in diameter or smaller. (c) SEM image of Bi_2Te_3 nanowires prepared using 90 electrodeposition/stripping cycles.

formed on them can be a millimeter in length (i.e., the diameter of a columnar grain in the HOPG crystal). However, long nanowires are obtained only after the coalescence of Bi_2Te_3 nuclei has proceeded to completion along each step edge. Our data show that the smallest Bi_2Te_3 nanowires that are continuous over distances of more than 100 μm are 60−80 nm in diameter. The individual Bi_2Te_3 crystallites comprising each nanowire can be observed in higher magnification SEM images, like those shown in Figure 3b and c.

Once nanowires are formed by the coalescence of these crystallites, the deposition of additional Bi_2Te_3 serves to increase the diameter of the nanowires. The diameter of the Bi_2Te_3 nanowires that are produced is a function of the number of growth cycles, *n*, as shown in Figure 4a. The populations of nanowires produced in a particular synthesis experiment are narrowly distributed in diameter, with a relative standard deviation of the diameter (RSD_{dia}) that ranged from 10 to 20%, as shown in the histograms plotted in Figure 4b−e. The granular morphology of these Bi_2Te_3 nanowires leads, frequently, to the presence of constrictions (circled regions in Figure 4b) of 20 nm or less at interparticle boundaries. This morphology contrasts with the smooth, cylindrical Bi_2Te_3 wires that are usually obtained in a template synthesis experiment.[16,18,19,33−35]

An attribute of the cyclic electrodeposition/stripping method is its propensity to produce material that is close to stoichiometric. EDX elemental analysis of Bi_2Te_3 nanowires (Figure 5a) shows them to be slightly tellurium rich with a Bi/Te ratio of 2:3.4, in agreement with the composition predicted from the Bi−Te phase diagram.[36] XRD analysis (Figure 5b) further confirms that the deposited material is the hexagonal phase of Bi_2Te_3. However, diffractions corresponding to out-of-plane periodicities, including 110, 205, 116, and 125, are more intense than expected for isotropically distributed crystallites relative to 015, and in-plane periodicities 1010 and 1115 are weaker than expected. As XRD is most sensitive to the out-of-plane periodicities, this skewing means that a crystallographically preferred growth direction exists along 110. This conclusion is supported by selected

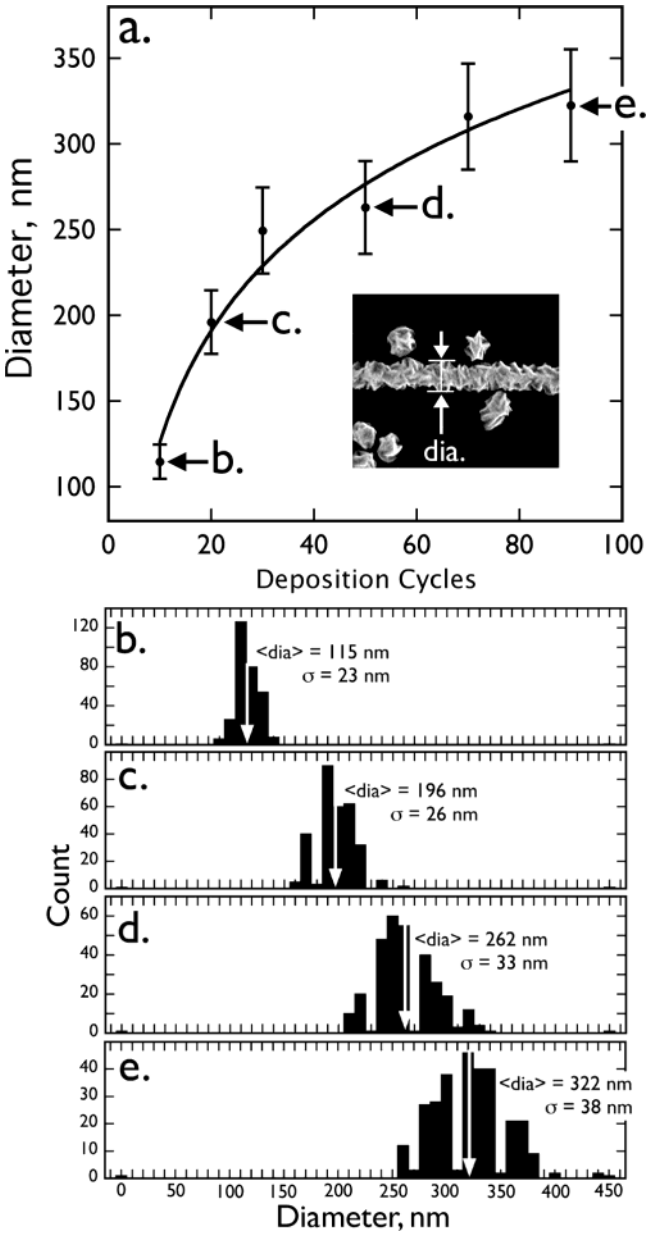

Figure 4. (a) Plot of the diameter of Bi_2Te_3 nanowires as a function of the number of electrodeposition/stripping cycles, *n*. The diameter plotted here is the outermost diameter of these nanowires, measured as indicated in the SEM image (inset). The diameter error bars shown in this plot represent $+1\sigma$ for the diameter measured from ≈300 nanowires. (b,c,d,e) Histograms of the outermost diameter for nanowires prepared using 10, 20, 50, and 90 electrodeposition/stripping cycles, *n*, respectively.

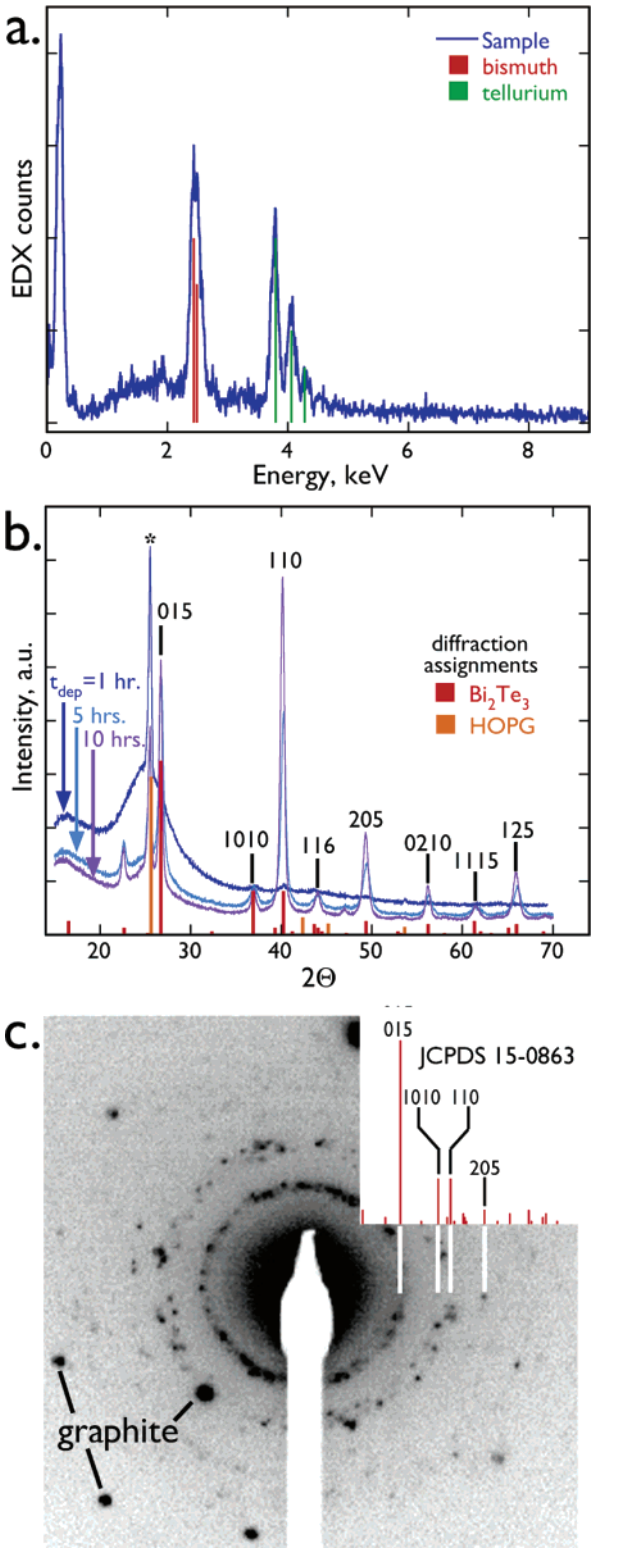

Figure 5. (a) Energy-dispersive X-ray fluorescence (EDX) for Bi_2Te_3 nanowires prepared by cyclic electrodeposition/stripping. The Bi/Te ratio calculated from this spectrum is 2:3.4 corresponding to 63 atomic percent tellurium, within the expected range based on the Bi−Te phase diagram.[36] (b) Powder X-ray diffraction for three Bi_2Te_3 samples prepared by cyclic electrodeposition/stripping for 1 h, 5 h, and 10 h. The 5 and 10 h samples were continuous films of Bi_2Te_3, whereas the 1 h sample consisted of wires with a mean diameter of approximately 500 nm. (c) Selected area electron diffraction pattern for a Bi_2Te_3 nanowire synthesized using cyclic electrodeposition/stripping.

area electron diffraction (SAED) which, in contrast to XRD, is most sensitive to in-plane periodicities. In the SAED pattern of Figure 5c the 205 reflection is absent (the diffraction spot shown there derives from graphite), but 015 is observed and consistent with hexagonal Bi_2Te_3.

We have demonstrated that cyclic electrodeposition/stripping can be coupled with step edge decoration to produce Bi_2Te_3 nanowires size-selectively. Uniquely, this method is capable of producing Bi_2Te_3 nanowires that are up to 1 mm in length and organized into parallel arrays of hundreds of wires. In future investigations, we are interested in under-

standing whether the crystallographic disorder present in these nanowires, coupled with the presence of narrow interparticle constrictions, enhances $S^2\sigma/\kappa$ and increases ZT.

Acknowledgment. This work was funded by the NSF (grant DMR-0405477). The authors thank Dr. Art Moore, formerly of GE Advanced Ceramics Inc., for donations of graphite, and they thank Prof. Derek Dunn-Rankin of UCI Mechanical and Aerospace Engineering for helpful discussions.

References

(1) Rowe, D. M. *CRC Handbook of Thermoelectrics*; CRC Press: London, 1995.
(2) Broido, D. A.; Reinecke, T. L. *Appl. Phys. Lett.* **1995**, *67*, 100.
(3) Broido, D. A.; Reinecke, T. L. *Phys. Rev. B* **1995**, *51*, 13797.
(4) Hicks, L. D.; Dresselhaus, M. S. *Phys. Rev. B* **1993**, *47*, 12727.
(5) Hicks, L. D.; Dresselhaus, M. S. *Phys. Rev. B* **1993**, *47*, 16631.
(6) Hicks, L. D.; Harman, T. C.; Dresselhaus, M. S. *Appl. Phys. Lett.* **1993**, *63*, 3230.
(7) Balandin, A. *Phys. Low-Dimens. Str.* **2000**, *1*−*2*, 1.
(8) Balandin, A.; Wang, K. L. *Phys. Rev. B* **1998**, *58*, 1544.
(9) Balandin, A.; Wang, K. L. *J. Appl. Phys.* **1998**, *84*, 6149.
(10) Walkauskas, S. G.; Broido, D. A.; Kempa, K.; Reinecke, T. L. *J. Appl. Phys.* **1999**, *85*, 2579.
(11) Zou, J.; Balandin, A. *J. Appl. Phys.* **2001**, *89*, 2932.
(12) Sur, I.; Casian, A.; Balandin, A. *Phys. Rev. B* **2004**, *69*.
(13) Martin, C. R. *Science* **1994**, *266*, 1961.
(14) Martin, C. R. *Chem. Mater.* **1996**, *8*, 1739.
(15) Hulteen, J. C.; Martin, C. R. *J. Mater. Chem.* **1997**, *7*, 1075.
(16) Sapp, S. A.; Lakshmi, B. B.; Martin, C. R. *Adv. Mater.* **1999**, *11*, 402.
(17) Martin-Gonzalez, M. S.; Prieto, A. L.; Gronsky, R.; Sands, T.; Stacy, A. M. *J. Electrochem. Soc.* **2002**, *149*, C546.
(18) Sander, M. S.; Prieto, A. L.; Gronsky, R.; Sands, T.; Stacy, A. M. *Adv. Mater.* **2002**, *14*, 665.
(19) Sander, M. S.; Gronsky, R.; Sands, T.; Stacy, A. M. *Chem. Mater.* **2003**, *15*, 335.
(20) Magri, P.; Boulanger, C.; Lecuire, J. M. *J. Mater. Chem.* **1996**, *6*, 773.
(21) Min, G. O.; Rowe, D. M. *J. Power Sources* **1992**, *38*, 253.
(22) Rowe, D. M.; Min, G. *IEEP*−*Sci. Meas. Tech.* **1996**, *143*, 351.
(23) Min, G.; Rowe, D. M. *Energy Convers. Manage.* **2000**, *41*, 163.
(24) The values of the quantities entering eq 2 were either measured from devices prepared in this laboratory (e.g., r_c) or were taken from the literature. These are as follows: $r = 10 \times 10^{-6}$ mm, $S = 2.00 \times 10^{-4}$ mV/K, $\Delta T = 25$ K, $\rho_c = 7$ kΩ, $\rho = 0.01$ Ω, and $L_c = 0.5$ mm. These values, taken from ref 1, are considered to be typical of state-of-the-art devices.
(25) Zach, M. P.; Ng, K. H.; Penner, R. M. *Science* **2000**, *290*, 2120.
(26) Favier, F.; Walter, E. C.; Zach, M. P.; Benter, T.; Penner, R. M. *Science* **2001**, *293*, 2227.
(27) Walter, E. C.; Favier, F.; Penner, R. M. *Anal. Chem.* **2002**, *74*, 1546.
(28) Penner, R. M. *J. Phys. Chem. B* **2002**, *106*, 3339.
(29) Walter, E. C.; Murray, B. J.; Favier, F.; Kaltenpoth, G.; Grunze, M.; Penner, R. M. *J. Phys. Chem. B* **2002**, *106*, 11407.
(30) Walter, E. C.; Murray, B. J.; Favier, F.; Penner, R. M. *Adv. Mater.* **2003**, *15*, 396.
(31) Li, Q.; Newberg, J. T.; Walter, E. C.; Hemminger, J. C.; Penner, R. M. *Nano Lett.* **2004**, *4*, 277.
(32) Kressin, A. M.; Doan, V. V.; Klein, J. D.; Sailor, M. J. *Chem. Mater.* **1991**, *3*, 1015.
(33) Prieto, A. L.; Martin-Gonzalez, M.; Keyani, J.; Gronsky, R.; Sands, T.; Stacy, A. M. *J. Am. Chem. Soc.* **2003**, *125*, 2388.
(34) Martin-Gonzalez, M.; Prieto, A. L.; Knox, M. S.; Gronsky, R.; Sands, T.; Stacy, A. M. *Chem. Mater.* **2003**, *15*, 1676.
(35) Prieto, A. L.; Sander, M. S.; Martin-Gonzalez, M. S.; Gronsky, R.; Sands, T.; Stacy, A. M. *J. Am. Chem. Soc.* **2001**, *123*, 7160.
(36) Okamoto, H.; Tanner, L. E. "Bi−Te (Bismuth-Tellurium) Phase Diagram," ASM, 1986.

NL048627T